Electronic Supplementary Material (ESI) for Soft Matter.

Supporting Information

Multi-stimuli-responsive actuator based on bilayered thermoplastic film

Mengdi Sun, Panlong Wang, Guoqiang Zheng*, Kun Dai, Chuntai Liu[1], Changyu Shen

College of Materials Science and Engineering, Key Laboratory of Material Processing and Mold (Ministry of Education), Henan Key Laboratory of Advanced Nylon Materials and Application, Zhengzhou University, Zhengzhou 450001, China

* Email address: gqzheng@zzu.edu.cn (G. Zheng.)

Supplementary Figures

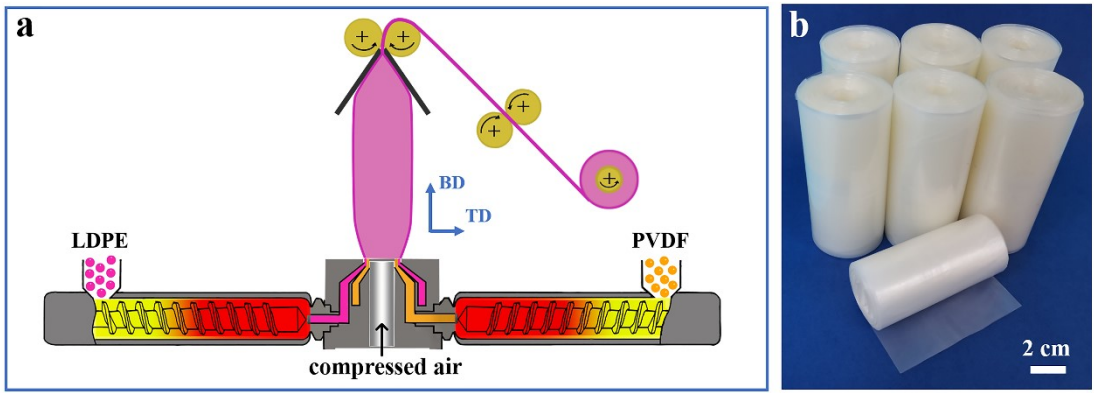

Fig. S1. (a) Schematic showing the method for fabricating PVDF/LDPE bilayered films. (b) Digital photo showing the roll-up PVDF/LDPE bilayered films. Scale bar: 2 cm.

Polyvinylidene fluoride (PVDF) and low density polyethylene (LDPE) particles were dried at 80 °C for 12 h. And then, it was blown into bilayered film using a bilayered film blowing machine (SCM50, Zhangjiagang Lianjiang Machinery Co., Ltd.) once the melt leaves the ring-shaped die (see Fig. S1a). One layer of the as-prepared PVDF/LDPE bilayered film was pure LDPE phase but the other layer was pure PVDF phase. The blowing up direction and transverse direction are marked as BD and TD, respectively. The take-up rate was 30 cm/min. The rolls of PVDF/LDPE bilayered films is shown in Fig. S1b, indicating the scalability of such fabrication method.

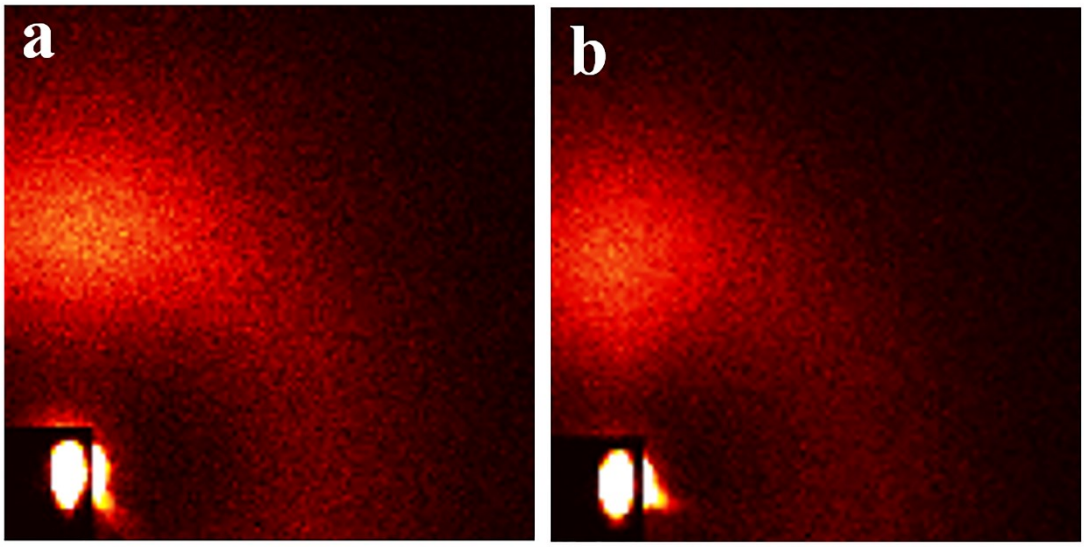

Fig. S2. 2D-SAXS patterns of (a) PL1 (ratio of the thickness for PVDF layer to that for LDPE layer was 5:1), (b) PL2 (ratio of the thickness for PVDF layer to that for LDPE layer was 1:5). The blowing up direction is horizontal.

To further determination of the orientation level, two-dimensional small-Angle X-ray scattering (2D-SAXS) measurement was conducted on a NanoinXider vertical systems (Xenocs, Sassenage, France) whose radiation wavelength of X-ray was 0.154 nm. Two-dimensional Dectris Platius hybrid pixel detector was employed to collect 2D-SAXS patterns. As shown in Fig. S2a, b, 2D-SAXS pattern of bilayered film displays a concentrated spot in meridional direction, indicative of high orientation level.

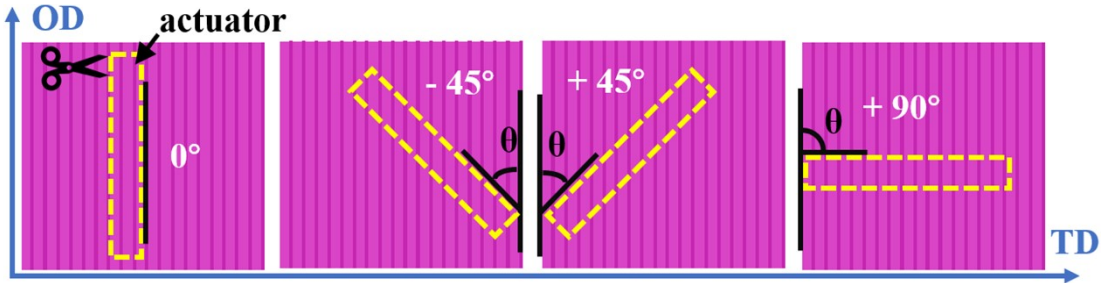

Fig. S3. Schematic images of the strips cut from PVDF/LDPE bilayered film. The orientation direction and transverse direction are marked as OD and TD, respectively.

The actuators (30 mm × 3 mm) were cut from the pristine PL1. It is worth noting

that θ is the angle between orientation direction (OD) and the long axis direction of the actuator.

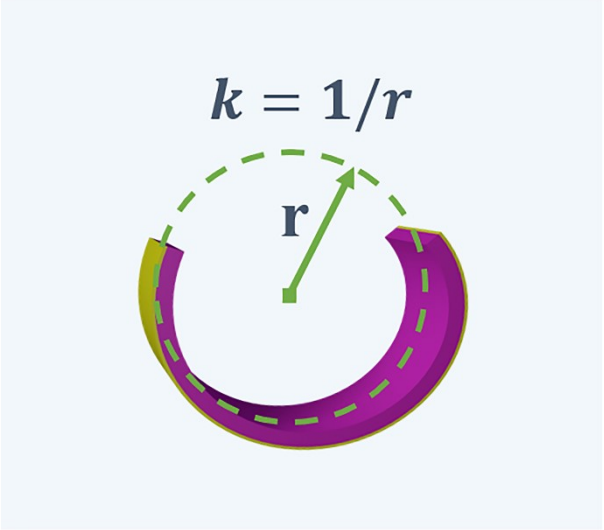

Fig. S4. Schematic showing the relationship between curvature (k) and radius (r).

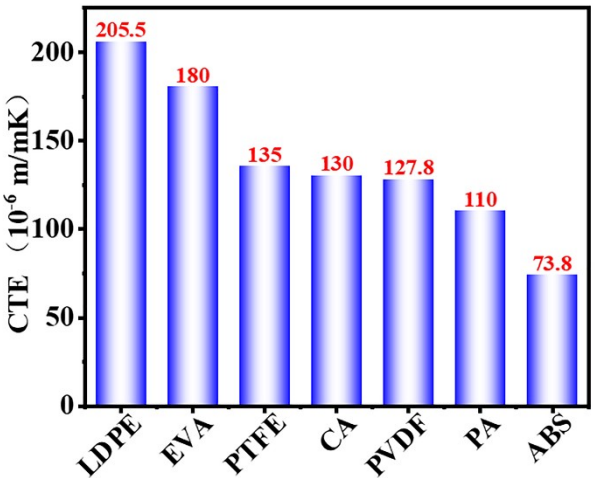

Fig. S5. Coefficient of thermal expansion (CTE) of typical common polymers [1, 2].

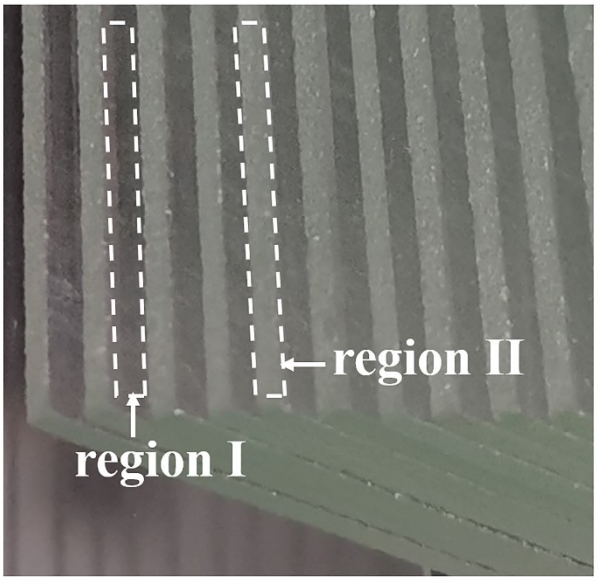

Fig. S6. Digital photo showing the different surface features.

Obviously, the surface of region I is very smooth while the surface of region II is relatively rough. Therefore, μ_2 in region II is definitely larger than μ_1 in region I, leading to the fact that $f_2 > f_1$.

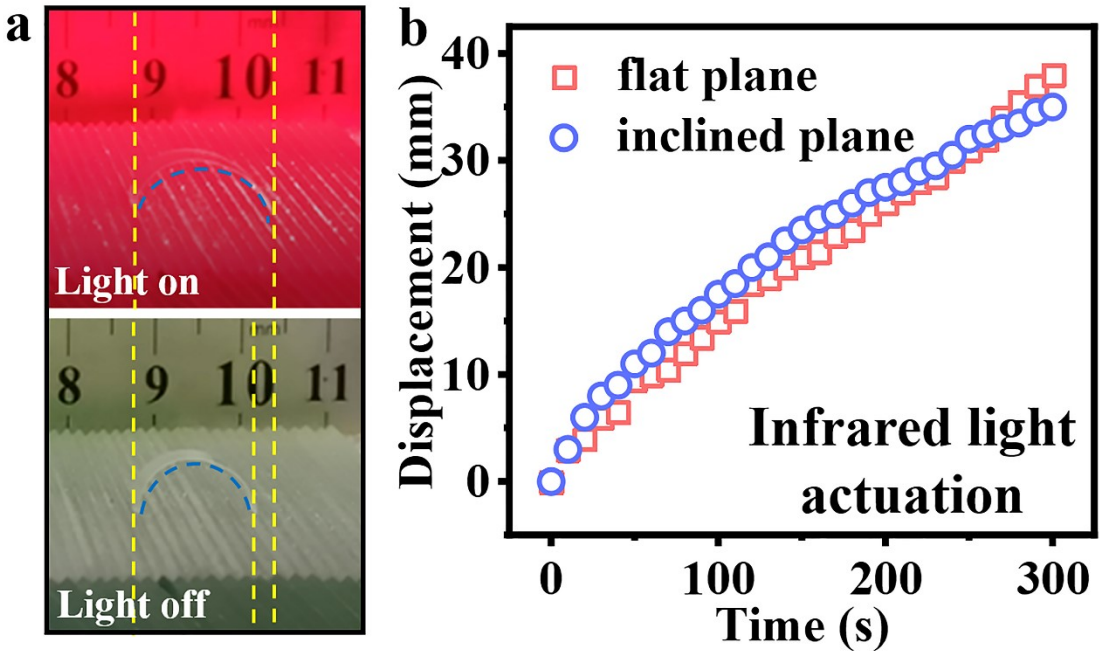

Fig. S7. (a) Consecutively captured images showing the worm-like self-walker crawling on dentate flat plane under infrared light. (b) Displacement as a function of time for the infrared light actuated worm-like self-walker.

Upon infrared light stimulation, worm-like self-walker based on PL2A (10 mm × 20 mm) with θ = 0° can also perform a worm-like crawl. Its two legs move apart when the light is on and move closer when the light is off (see Fig. S7a). The displacement-time curve is shown in Fig. S7b. The worm-like self-walker can also move about 35 mm in 300 s. It can be seen from the slope that the worm-like self-walker is generally of the same crawling speed.

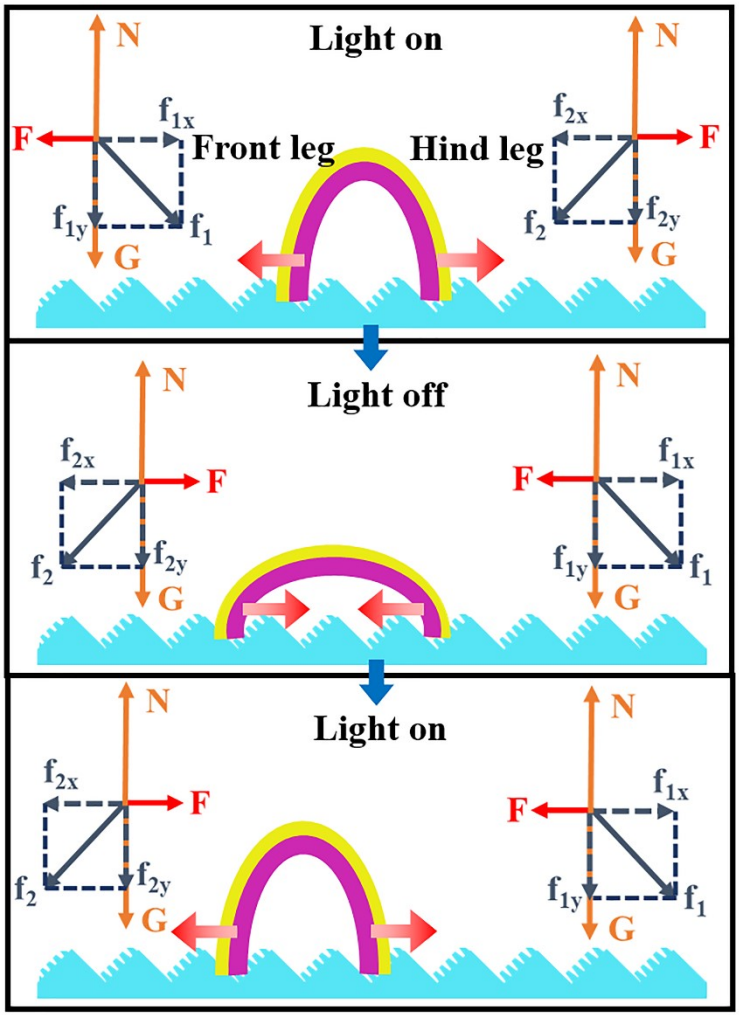

Fig. S8. Schematic diagram showing force analysis of the worm-like self-walker under infrared light.

The schematic diagram showing force analysis of the worm-like self-walker under infrared light is presented in Fig. S8, which is similar to that actuated by acetone vapor.

When the worm-like self-walker is exposed to infrared light, the two legs move apart and their driving forces (red arrow) are the same. The maximum friction of front leg acting on region I (f_1) can be resolved into horizontal component force f_{1x} and vertical component force f_{1y}. The maximum static friction of hind leg acting on region II (f_2) can be resolved into horizontal component force f_{2x} and vertical component force f_{2y}. Hence, when the driving force (F) is smaller than f_{1x} but larger than f_{1x} (i.e., $f_{1x} > F > f_{2x}$), the hind leg remains stationary while front leg moves forward. Then, when infrared light is off, the two legs move closer and the driving forces (red arrow) of two legs are equal. At this moment, the maximum friction of front leg acting on region II is f_2 while the maximum static friction of hind leg acting on region I is f_1. Hence, the front leg remains stationary while hind leg moves forward. As a result, the repeated bending and extension of the two legs can be converted into a forward motion.

Supplementary Videos

Video S1. The worm-like self-walker based on PL1 soft actuator crawling on a dentate flat upon acetone vapor stimulation.

Video S2. The worm-like self-walker based on PL1 soft actuator crawling on a dentate plane with inclination of 20° upon acetone vapor stimulation.

Video S3. The worm-like self-walker based on PL2 soft actuator crawling on a dentate flat upon infrared light stimulation.

Video S4. The worm-like self-walker based on PL2 soft actuator crawling on a dentate plane with inclination of 20° upon infrared light stimulation.

Video S5. The crawler-type robot based on PL2 soft actuator rolling on a flat surface.

Video S6. The crawler-type robot based on PL2 soft actuator climbing steps.

Video S7. The actuation behavior of PL2 soft actuator upon human palm temperature stimulation.

Video S8. The smart gripper based on PL2 soft actuator picking up and moving a cuboid polymer foam.

References

[1] L. Li, J. Meng, C. Hou, Q. Zhang, Y. Li, H. Yu and H. Wang, *ACS Appl. Mater. Interfaces*, 2018, **10**, 15122-15128.

[2] S. Zhou, F. Cun, Y. Zhang, L. Zhang, Q. Yan, Y. Sun and W. Huang, *J. Mater. Chem. C.*, 2019, **7**, 7609-7617.